Technical Note

Development of a novel maglev positioner with self-stabilizing property

Kwang Suk Jung [a,*], Yoon Su Baek [b]

[a] *Mechanical Engineering Department, Graduate School, Yonsei University, 134 Shinchon-dong, Sudaemun-ku, Seoul, 120-749, South Korea*
[b] *School of Electrical and Mechanical Engineering, Yonsei University, 134 Shinchon-dong, Sudaemun-ku, Seoul, 120-749, South Korea*

Abstract

This paper presents a novel six degrees of freedom (d.o.f) maglev positioner devoid of mechanical friction which is one of the most severe factors that limit the resolution of a system. One moving part levitated magnetically over fixed element is an inherently unstable, namely open-loop unstable. And the magnetic force acting on the levitated part is nonlinear in nature. Then the system requires a considerably computational load in the control aspect to compensate the instability and nonlinearity of rigid body in space, and to achieve the satisfactory performance. Therefore, we have focused on realizing self-stability with a minimum feedback signal and optimized principal parameters to obtain high disturbance rejection property of the uncontrolled d.o.f with only the passive stability. It means that we can care for a performance of the controlled d.o.f without considering the stability of the uncontrolled d.o.f. We demonstrate that it is possible for the system to achieve the desired performance with feedback of just a position signal via the experiments. © 2002 Elsevier Science Ltd. All rights reserved.

Keywords: Magnetic levitation; Self-stability; Superposed solution; Free vibration; Step input control; Optimization; Dynamic formulation

1. Introduction

With the challenge of the shrinking dimension in fabrication process in recent years, demands are growing for high precision and repeatability. Practically, wafer

---

* Corresponding author. Tel.: +82-02-2123-4407; fax: +82-02-362-2736.
  E-mail address: jungks@yonsei.ac.kr (K. Suk Jung).

stepper stages for photolithography and probing stations, which are used to probe electronically either the interior of ICs or the IC bond pads, require increasingly precise multi-degrees of freedom (d.o.f) motions. Additionally, the probing stations will have to control force to ensure that the probe contact does not scratch the device under testing, as well as motion of the probe tip to keep up with greater density of ICs. Therefore, magnetic suspension techniques (MST) replacing the existing functional elements such as piezo and shape memory alloy are being studied actively to realize the above performance [1,2]. As mentioned above, in case the delicate force control as well as the fine motion control of high precision system is required, MST make it possible to control a force comparatively simply without force transducer as the measured gap information can be transformed into force by a simple calibration [3–5].

The earliest developments in MST can be traced to contactless magnetic bearings and levitated trains, examples of narrow gap devices in which the control problem was one of regulation to a desired setpoint [6–8]. Current technology in MST is based on the same narrow gap principle, except that the control problem is to provide tracking of the actuator endpoint within the confines of a limited region around a nominal operating point [9,10]. Tracking performances of devices utilizing MST are becoming more important because they are being applied to semiconductor manufacture and inspection such as wafer stepper and probing stage [4,11].

The major advantage of levitation is that the levitated devices can be regarded as a rigid body devoid of jointed parts, and then friction can be dramatically reduced. It means that the position errors are not accumulated, the dynamic behavior is simple to model, the fabrication is straightforward, and harsh environments do not pose a problem since the device can be coated. And MST are highly suited for semiconductor production line which requires clean-room environment as the levitated part does not generate wear particles [4,11–13]. Apart from various advantages, they require a considerably computational load in the control aspect to compensate the instability of rigid body in space. And the levitated part is open-loop unstable and uncontrolled between sampling instants. Thus it "run away" during the interval in which the control current is held constant. Therefore, the existing devices have required the controller of high performance and bandwidth to achieve the precise motion, and considered the stability as the most important factor in control logic.

In this paper, we introduce a novel six d.o.f maglev positioner capable of being levitated stably with a minimally sensory feedback in space and confirm the passive stability of the uncontrolled d.o.f through dynamic formulation and experiment. To overcome problems of MST stated above, we have focused our design effort on the realization of the self-stability with a minimum feedback position signal of levitated part. But, because the uncontrolled d.o.f motions have just passive stability, they must have high stiffness under a constant input to keep performance of controlled d.o.f motion. Then, it is necessary to decide the principal parameters through optimization, which results in more improved robustness to the external disturbance.

This paper is organized as follows. In Section 2, we discuss the magnetic theory, model the stiffness and damping effects resulting from the interaction between the used magnetic pair, and compare the proposed theory with the experiment.

In Section 3, we design a maglev positioner, derive the dynamic formulation, and optimize the principal parameters to maximize damping and stiffness coefficients in all d.o.f. To verify stability and dynamic formulation of the proposed positioner, and to quantify the influence of coupling due to the uncontrolled d.o.f on the controlled d.o.f, we provide experimental results in Section 4. A simple linear control method is discussed over there. Section 5 summarizes the work performed in this research and discusses future work.

2. Theoretical formulation of magnetic force

As magnetic systems are inherently nonlinear and difficult to model in most cases, it is desirable to choose magnetic elements excluding factors difficult to quantify, in order to realize a micromotion repeatedly without accumulation of error. A promising magnetic structure utilizes permanent magnets on the moving stage which are driven by air-core solenoids, which have no hysteresis caused by ferromagnetic materials, no eddy current loss, and no flux saturation, in the fixed machine base. The magnetic phenomena by interaction of the elements are discussed in this section.

2.1. Force characteristic of air core solenoid

In Fig. 1, the force and the torque on a permanent magnet (PM), assumed to be the *z*-directed magnetic dipole moment, can be expressed in terms of the external magnetic field density *B* and its gradient as [14]
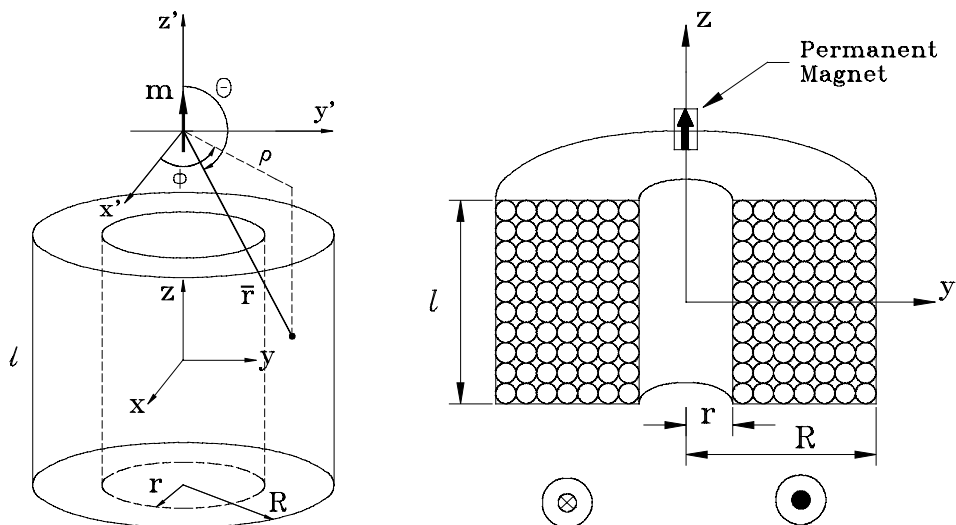

Fig. 1. Air-core solenoid superposed with current loops.

$$F = (m_z \cdot \nabla)B \quad \text{or} \quad F_n = m_z \frac{\partial B_n}{\partial z}, \tag{1}$$

$$T = m_z \times B = m_z B_x j - m_z B_y i, \tag{2}$$

where m_z is the magnetic dipole moment and n is x, y, z. Then, the calculation of the magnetic forces results in the quantification of the magnetic field density. The magnetic field density produced by a steady current density flowing in a closed circuit can be generally expressed by the Biot–Savart law. Based on the law, we can calculate the magnetic field density, B, of the arbitrary point on the central axis(z) of a current loop as [14]

$$B_z = \frac{\mu_0 I a^2}{4\pi(a^2 + z^2)^{3/2}} \int_0^{2\pi} \mathrm{d}\phi = \frac{\mu_0 I a^2}{2(a^2 + z^2)^{3/2}}, \tag{3}$$

where μ_0 is the permeability of empty space, a the radius of the loop, and I the current flowing in the loop. But the multi layer air-core solenoid proposed in this paper has a structure superposing a sequence of circular current loops in the axial direction and then in the radial direction like Fig. 1. However, there exists no explicit formulation to express the magnetic field density for an arbitrary point of the multi layer air-core solenoid. But we can obtain an approximate solution through superposing N times the magnetic field density which a current loop produces, as the multi layer air-core solenoid can be assumed to the superposed form of current loops with an equivalent radius. Therefore, integrating the magnetic field density given in (3) in radial and longitudinal directions, calculating its mean value, and then multiplying by coil turns no., we get the entire magnetic field density. As coil turns no. of solenoid is large, this is a suitable approximation. It is like

$$B_z = \frac{\mu_0 N I}{2l(R - r)} \left[\left(z + \frac{l}{2}\right) \ln \frac{R + \sqrt{R^2 + (z + l/2)^2}}{r + \sqrt{r^2 + (z + l/2)^2}} \right.$$
$$\left. + \left(z - \frac{l}{2}\right) \ln \frac{r + \sqrt{r^2 + (z - l/2)^2}}{R + \sqrt{R^2 + (z - l/2)^2}} \right], \tag{4}$$

where N is coil turns no. and l, R, r are dimensions of the solenoid described in Fig. 1.

2.2. Modeling of electromotive force due to PM's movement

The electromotive force (emf) is induced in the solenoid by up-down motion of PM that interacts with air-core solenoid as Fig. 1. This emf is generally generated by change of the magnetic flux due to the motion of the circuit or PM, and due to the time dependence of the field. In addition, if induced current flows, it will be in such a direction that the magnetic field it produces tends to counteract the change in flux that induces the emf. Therefore, the emf in physical system results in the damping

effect. In case the PM is approximated by a magnetic dipole moment, the emf induced in the air-core solenoid by up-down motion of the PM in the z-direction (see Fig. 1) can be expressed in terms of the vector potential 'A' easily. When the PM is put on the origin, points toward the z-axis (Fig. 1), we get the electromotive force induced in a current loop at the distance $\bar{r}$ apart from the origin of PM by the vector potential at a point (ρ, θ, ϕ) as follows [14]:

$$\varepsilon_z = -\frac{\partial \Phi}{\partial z}\frac{\partial z}{\partial t} = -\frac{d}{dt}\int_c A \, dl = -\frac{d}{dt}\left[\frac{\mu_0 m_z \rho^2}{2(z'^2 + \rho^2)^{3/2}}\right]. \tag{5}$$

But in case of the air-core solenoid, the magnitude of magnetic flux induced in current loops constituting the solenoid varies according to their relative position to the PM. Therefore, superposing the flux (square bracket in (5)) produced by a current loop in radial and longitudinal direction similarly with the derivation of the magnetic field density, we get the entire magnetic flux of the solenoid. In case of that the distance from (x, y, z) to (x', y', z') is $l/2$, it is (see Fig. 1)

$$\Phi(z) = \frac{\mu_0 m_z N}{2(R-r)l}\left[\left(z - \frac{l}{2}\right)\ln\frac{r + \sqrt{r^2 + (z-l/2)^2}}{R + \sqrt{R^2 + (z-l/2)^2}} + \left(z + \frac{l}{2}\right)\ln\frac{R + \sqrt{R^2 + (z+l/2)^2}}{r + \sqrt{r^2 + (z+l/2)^2}}\right]. \tag{6}$$

Above result takes a very similar form with (4), the approximated solution of the magnetic field density. This is caused by assumption that the PM is a magnetic dipole moment. As m_z is $I \times S$, in which S is a coil loop area, and a magnetic field density is a magnetic flux per unit area, the consistent feature in the derived equations is observed. Induced current, flowing in the coil by the change of the flux generated in (6), produces another magnetic field again. Then, a total magnetic flux of system $\Psi(z, i)$ is the sum of a magnetic flux $\Phi_m(z)$ by the PM like (6), under the assumption of a constant magnetic dipole moment, and a magnetic flux $\Phi_l(i)$ by the induced current unrelated to the PM. If u is the voltage applied across coils having a resistance of $R\Omega$ we get the voltage equation like

$$u = iR + \frac{d\Psi}{dt} = iR + \frac{d}{dt}(\Phi_m + \Phi_l) = iR + \frac{\partial \Phi_m}{\partial z}\frac{\partial z}{\partial t} + L\frac{di}{dt}, \tag{7}$$

where L is the self-inductance of coils. As the applied voltage is zero in the above equation, an induced current flowing in the coil can be calculated substituting (7) for (5). By the interaction of the magnetic fields generated by the induced current and the PM, a damping force such as (8) acts on the PM on the basis of (1).

$$F_d = m_z\frac{\varepsilon_z}{R}(1 - e^{-t/\tau})\frac{\partial}{\partial i}\left(\frac{\partial B_z}{\partial z}\right), \tag{8}$$

where τ means an induced time constant, L/R.

2.3. Experimental verification of theoretical modeling

To verify the approximate solutions derived by superposition in last section, we carried out experiments for two air-core solenoid models. As the magnetic field density by an assigned current takes a similar form with the magnetic flux by a magnetic dipole moment, an experiment for only one has been performed. And we have decided to measure the magnetic force (1) rather than the magnetic filed density (4) for later usefulness. Specifications of the two used solenoid models, r, R, l, N, are 8, 18.1, 24.6 mm, 993 and 8, 18.35, 23.8 mm, 970, respectively, and the advanced neodymium–iron–boron rare earth PMs, which have strong coercive force (867,000 A/m) and high residual induction property, are selected. Theoretical modeling is based on result combining (1) and (4) and at this time, there is no torque generated because a direction of PM is assumed to coincide with one of the solenoids. But it is very difficult to get the closed form solution of a radial force on PM theoretically as described before, and then we show the only experimental results. They can make us confirm that it is possible to model linearly the radial force within the limited range. Fig. 2(a) and (b) show z position of the PM relative to the solenoid upper face versus axial forces on the PM for two models, where source currents are 0.5/1A. And Fig. 3(a) and (b) show radial position versus radial forces on the PM according to its axial position relative to the solenoid upper face, where currents are same with the above case. In the figures, the theoretical results are in very good agreement with the experimental data. Additionally by Figs. 2(a) and (b), we can infer that the force acting on the PM has the property of spring force when it puts inside rectangular dotted line. This feature fits in with condition that the divergence of external force is less than zero, and is a necessary condition for stability in the direction [8]. Calculating the self-inductance for the first model, we get $L = 0.000673H$. As the resistance of the coils is about 8 Ω, the induced time constant is 0.000084. Therefore, for the magnetic system proposed in this paper with a little inductance against resistance, there is no necessity for considering rising time of induced current. Practically, we can hardly identify the effect of rising time through simulation and know that the shape of induced emf poses a nearly square waveform through a simple experiment. Then, the damping force (8) can be assumed in this system as follows:

$$F_{\mathrm{d}} = m_z \frac{\varepsilon}{R} \frac{\partial}{\partial i} \left(\frac{\partial B_z}{\partial z} \right). \tag{9}$$

3. Magnetically levitated positioner – design, modeling, and optimization

In the last chapter, we confirmed that there exists an operating space, with property of spring, which guarantees stability in the axial direction of the system composed of air-core solenoid and PM. But this stability is not guaranteed any more in the radial direction of the solenoid. In addition, we know that it is impossible for a magnetic pole put under the static field to levitate stably [8]. Then, it is impossible for the rigid body in the space to sustain the stability for entire d.o.f without sensory
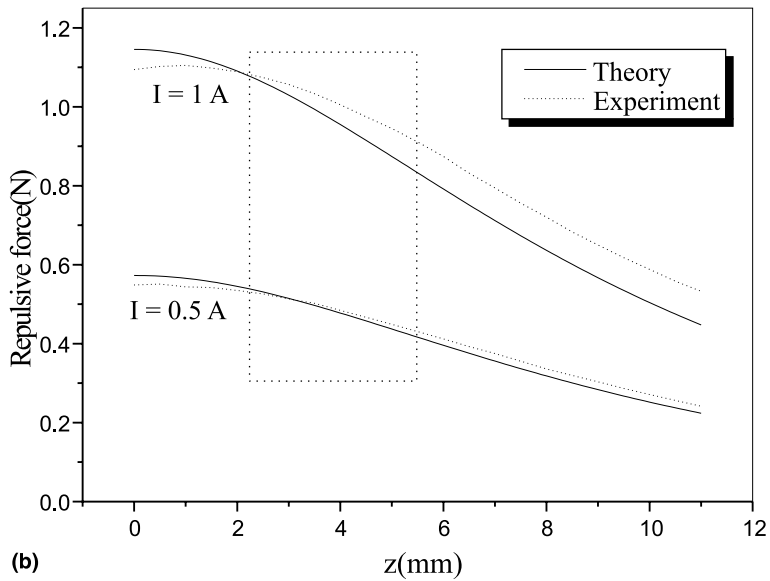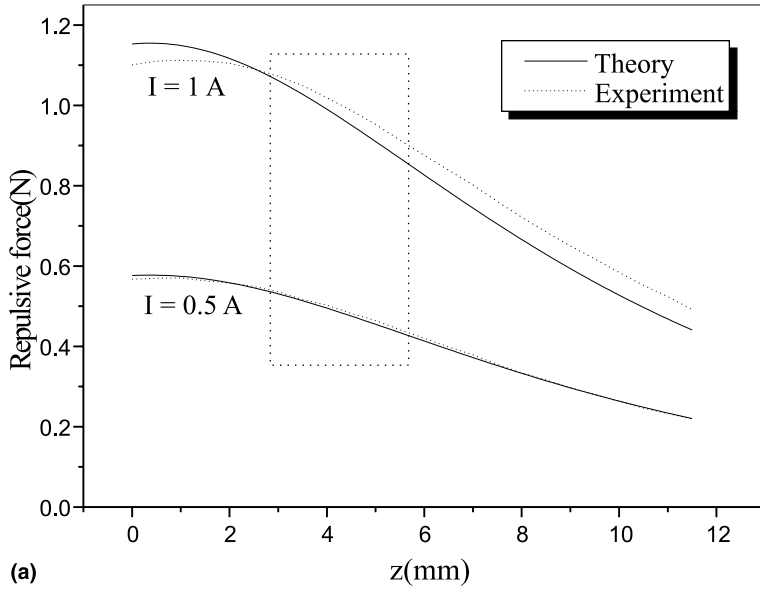
Fig. 2. (a) Axial force on PM for the first solenoid model. (b) Axial force on PM for the second solenoid model.

feedback. Therefore the out-of-plane motions (z, α, β) and the in-plane ones (x, y, γ) should be compounded properly, to secure the stability with a minimum sensory signal and to satisfy the necessary condition of self-stability. The entire configuration
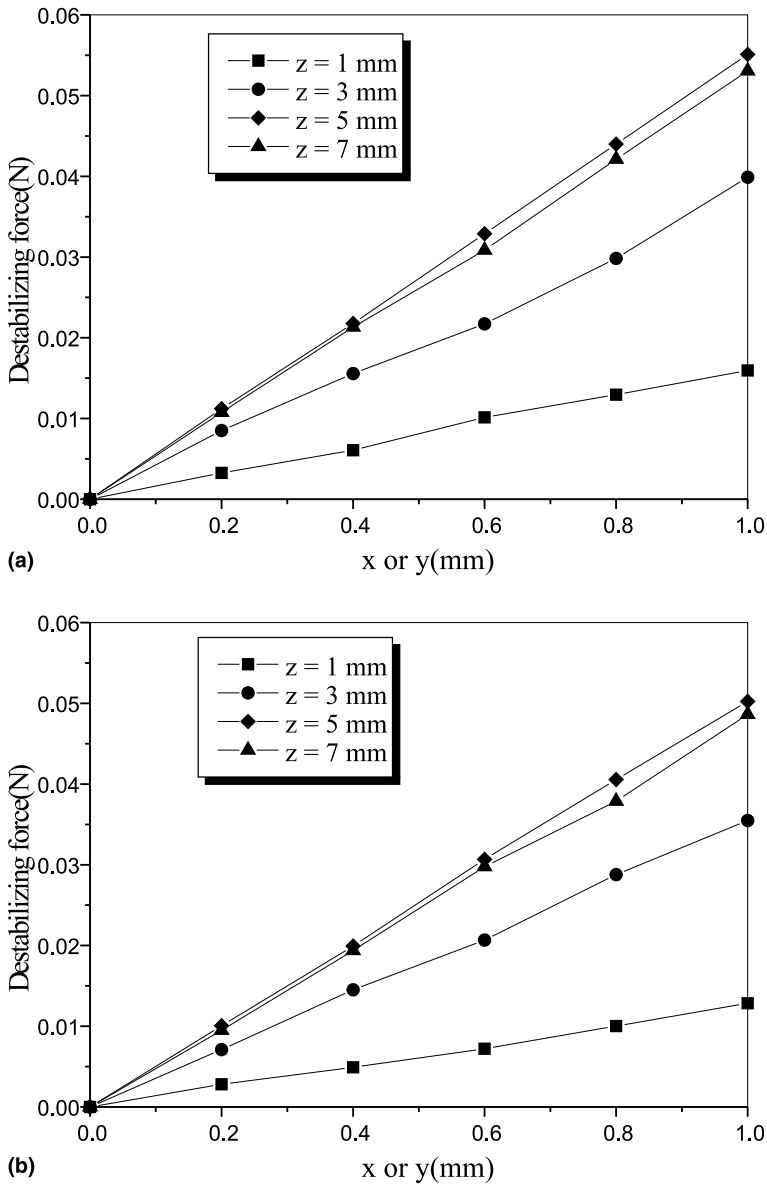
Fig. 3. (a) Radial force on PM for the first model. (b) Radial force on PM for the second model.

of magnetic positioning system that can guarantee the maximum stability is described in Fig. 4. In the figure, the rotor composed of PMs and the frames supporting them levitate over the stator composed of air-core solenoids by repulsive force as mentioned above. The combination is arranged to be able to generate repulsive forces on PMs in normal plane of levitating axis also. The special feature of this
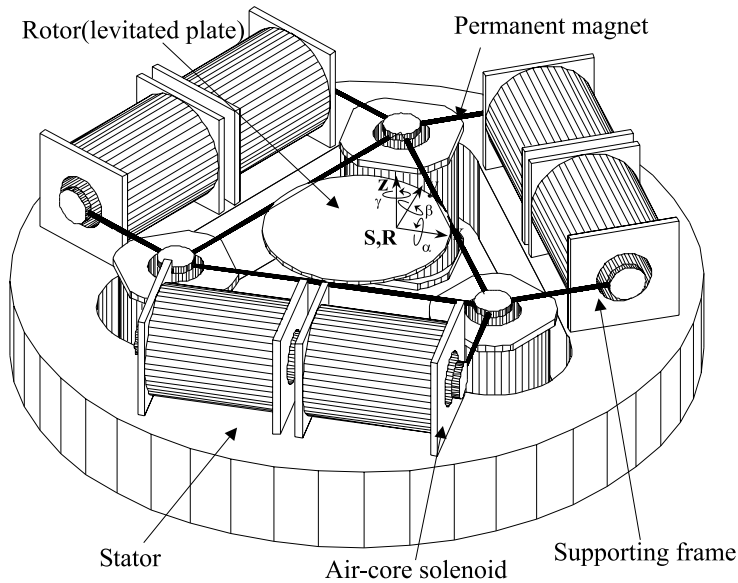
Fig. 4. Concept configuration to describe the force generating mechanism and the principle of six d.o.f realization, and global coordinate system of the proposed maglev positioner.

structure is that an arbitrary one d.o.f motion is stable under constraints of the other d.o.f motion. Of course, the rotor is levitated in free space without any constraint and is impossible to sustain the stability of entire d.o.f without feedback signal. The above feature means only that the system can secure self-stability of the other d.o.f so long as a position signal of at least one d.o.f feeds into the system.

3.1. Dynamic formulation of system

Let us make a dynamic analysis to verify stability for the entire system. The global and the local coordinate systems used in this analysis are shown in Figs. 4 and 5 and utilize the fixed angle criterion to specify an orientation. In Figs. 4 and 5, S and R represent base coordinate systems for each stator and rotor. And $A–F$ represent base coordinate systems of solenoids fixed in the stator frame, $am–fn$ do those of PMs. It is assumed that the origins of stator and rotor coincide and the axis of rotor is parallel with that of stator at initial time.

When the rotor takes a perturbation such as $(\delta X, \delta Y, \delta Z, \delta\alpha, \delta\beta, \delta\gamma)$ with respect to (wrt) stator, the forces obtained from the relationship of solenoid and PM can be expressed by stiffness force and damping force. Note that these narrow gap devices employ linear system analyses and control strategies that are based on a Taylor series expansion of the actual nonlinear force distribution at the nominal operating point. As the magnetic field density is a function of current i and position r, and the emf is a function of velocity $\dot{r}$ and r, the first variation of force is
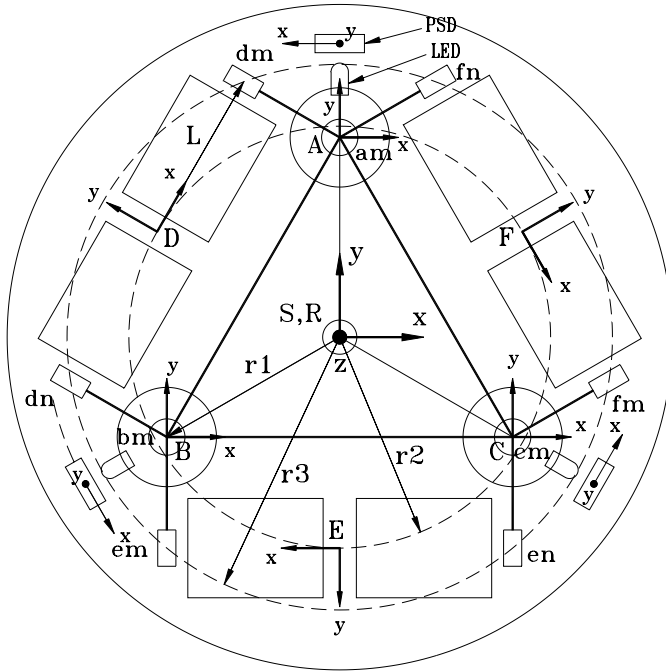
Fig. 5. Local coordinate system (upper view of configuration).

$$\delta F(\dot{r}, r, i) = \delta F_{\mathrm{d}}(\dot{r}, r) + \delta F_{\mathrm{s}}(r, i) = \frac{\partial F_{\mathrm{d}}}{\partial \dot{r}} \delta \dot{r} + \frac{\partial F_{\mathrm{s}}}{\partial r} \delta r + \frac{\partial F_{\mathrm{s}}}{\partial i} \delta i$$

$$= k_{\mathrm{d}r}|_{r=r_0} \delta \dot{r} + k_r|_{r=r_0, i=i_0} \delta r + k_i|_{r=r_0} \delta i, \tag{10}$$

where r_0 and i_0 represent nominal operating position, current, respectively. Spring force F_{s} is calculated by (1) and (3), and damping force F_{d} by (9). Here we neglect the influence of r on F_{d}. And $k_{\mathrm{d}r}$, k_r, k_i mean damping coefficient, stiffness coefficient, force constant in the r (i.e. x, y, z) direction. Actually,

$$k_r \text{ is } m_z \frac{\partial}{\partial z}\left(\frac{\partial B_z}{\partial z}\right),$$

$$k_{\mathrm{d}r} \text{ is } m_z \frac{\partial}{\partial \dot{z}}\left(\frac{\varepsilon_z}{R}\right)\frac{\partial}{\partial i}\left(\frac{\partial B_z}{\partial z}\right)$$

and

$$k_i \text{ is } m_z \frac{\partial}{\partial i}\left(\frac{\partial B_z}{\partial z}\right).$$

Then we can think that there are virtual springs and dampers between the solenoid and the PM in Fig. 4. For the case, an entire dynamic formulation can be derived easily through a conventional vibration system analysis. The cautious thing is that the magnitude of stiffness coefficient and force constant in the radial direction in (10)

is around or below 20% of ones in the axis direction within the operating range of rotor, 2 mm, as shown in the experimental results of Section 5. Expressing in more detail, the force generated in the radial direction of the electromagnet is not restoring force, namely unstable force as described. Thus, expressing the stiffness coefficient in the direction, its sign is minus. Then, the discussion of the coefficient in the direction is physically meaningless. The magnetic force in the radial direction of the electro-magnet is very small compared with that of the axis direction within the confined range, because the axis offset between the magnetic pair is around ±2 mm at most. Then, they are all selected into 0.2 times those of the axis direction and the damping force in the radial direction is neglected. And the weight of rotor is canceled by nominal currents of solenoids for out-of-plane motion, solenoids for in-plane motion and for out-of-plane motion have all the same specification, respectively, and identical PMs are used. Considering the direction cosines of the repulsive forces between the magnetic pair on the basis of the local frames in Fig. 5, all the magnetic forces can be described in the global frame. Then substituting (10) for their components, the entire dynamic formulations of the levitated plate can be derived easily because the system can be converted into an equivalent linear vibration system as mentioned above. Dynamic formulations removing variation 'δ' are (sub-index ip represents in-plane motion, op does out-of-plane motion)

$$m\ddot{X} + k_{dx}\dot{X} + k_x X = m\ddot{X} + 3k_{dip}\dot{X} + (2.4k_{ip} - 0.6k_{op})$$
$$= \frac{1}{2}k_{ipi}[(I_{dm} - I_{dn}) - 2(I_{em} - I_{en}) + (I_{fm} - I_{fn})],$$

$$m\ddot{Y} + k_{dy}\dot{Y} + k_y Y = m\ddot{Y} + 3k_{dip}\dot{Y} + (2.4k_{ip} - 0.6k_{op})Y$$
$$= \frac{\sqrt{3}}{2}k_{ipi}[(I_{dm} - I_{dn}) - (I_{fm} - I_{fn})],$$

$$m\ddot{Z} + k_{dz}\dot{Z} + k_z Z = m\ddot{Z} + 3k_{dop}\dot{Z} + (3k_{op} - 1.2k_{ip})Z = k_{opi}(I_A + I_B + I_C),$$

$$I_{xx}\ddot{\alpha} + k_{d\alpha}\dot{\alpha} + k_\alpha\alpha = I_{xx}\ddot{\alpha} + \frac{3}{2}r_1^2 k_{dop}\dot{\alpha} + \left(\frac{3}{2}r_1^2 k_{op} - 0.6(L^2 + r_2^2)k_{ip}\right)\alpha$$
$$= r_1 k_{opi}\left(I_A - \frac{1}{2}I_B - \frac{1}{2}I_C\right),$$

$$I_{yy}\ddot{\beta} + k_{d\beta}\dot{\beta} + k_\beta\beta = I_{yy}\ddot{\beta} + \frac{3}{2}r_1^2 k_{dop}\dot{\beta} + \left(\frac{3}{2}r_1^2 k_{op} - 0.6(L^2 + r_2^2)k_{ip}\right)\beta$$
$$= \frac{\sqrt{3}}{2}r_1 k_{opi}(I_B - I_C),$$

$$I_{zz}\ddot{\gamma} + k_{d\gamma}\dot{\gamma} + k_\gamma\gamma = I_{zz}\ddot{\gamma} + 6r_2^2 k_{dip}\dot{\gamma} + ((6r_2^2 - 1.2L^2)k_{ip} - 0.6r_1^2 k_{op})\gamma$$
$$= -r_2 k_{ipi}[(I_{dm} - I_{dn}) + (I_{em} - I_{en}) + (I_{fm} - I_{fn})]. \tag{11}$$

Here k_{ip}, k_{op} are stiffness coefficients, terms with sub-index including i, i.e. k_{ipi}, k_{opi} are force constants in the axis direction, and k_{dip}, k_{dop} are damping coefficients.

We can predict easily from (11) that the damping and the stiffness of entire d.o.f are positive values for k_{op} that is a little larger than k_{ip}. It means that the system is stable asymptotically. Namely, when the system is put in the nominal position, it has the self-stability in spite of external disturbances within a definite range. Of course, this is an inevitable result caused by assuming that there is no torque generated by misalignment of magnetic elements and neglecting this disturbance torque in a linear perturbation method which is the derivation procedure of equation of motion. Then, it is more reasonable to regard (11) as an independent dynamic equation of one d.o.f derived under constraints of the other d.o.f, not those of entire d.o.f. Namely, although each d.o.f has self-stability, the real system becomes unstable in the arbitrary direction, it depends on the initial condition, because of the disturbance torque. But as described previously, this system has the necessary condition for self-stability, and then it is possible to sustain the self-stability by just one or two sensory feedbacks. At that time, the dynamic characteristics of the other d.o.f motions are governed by (11).

3.2. Optimization of parameters

Under a constraint that a solenoid volume and an assigned current are fixed, a magnetic field density produced by the solenoid is in proportion to outer diameter of the solenoid, but its gradient has a maximum value in a certain dimension. Then there exists an optimum dimension of solenoid to maximize magnetic force from interacting with PM. In addition, the system which realizes the six d.o.f in terms of a compounding of in-plane motion and out-of-plane motion, as we know from the derived equations of motion, has a coupled form that the damping, stiffness coefficients of entire d.o.f are mixed with damping, spring constants of each element. And the uncontrolled d.o.f have just passive stability as described before. Therefore, all design variables should be chosen properly to cope with disturbances for any direction robustly. Then, it is essential to select the design parameters by the optimization procedure.

The design parameters to be determined through optimization procedure are dimensions of solenoid and values related to system configuration that maximizes the stiffness and the damping of six d.o.f under the limited currents and the fixed solenoid volumes. Then, the object function Φ for optimization of design is chosen as follows:

$$\min \Phi(d_i, D_i, l_i, z_i, I_i, r_2),$$

$$\Phi = \sum_{j=x,y,z,\alpha,\beta,\gamma} \frac{1}{k_j^2} + \sum_{j=dx,dy,dz,d\alpha,d\beta,d\gamma} \frac{1}{k_j^2} + \sum_{j=ipi,opi} \frac{1}{k_j^2}, \tag{12}$$

where design parameters d_i, D_i, l_i are an inner diameter, an outer diameter, a length of each solenoid, z_i nominal position of PM relative to solenoid, I_i nominal current, and r_2 distance from origin of stator to solenoid frame D, E, F. As i means an index of solenoids that take charge of in-plane motion and out-of-plane motion, there are 11 design parameters in all.

In the above object function, all the terms are referred to (10) and (11). The reason for inserting the last term into the object function is that the relative positions of
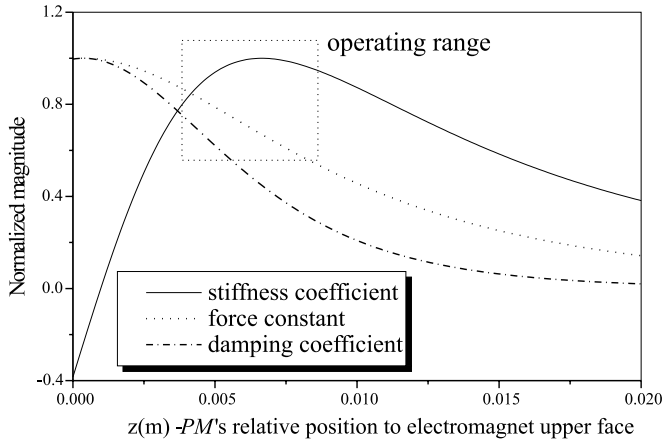
Fig. 6. Variation of each coefficient according to relative position of PM to solenoid.

solenoid to PM, which make force constant and stiffness coefficient maximize, are different from each other. Therefore, we perform the optimization considering two terms in all. In addition, the magnitude of stiffness coefficient is also in inverse proportion to one of damping coefficient according to the relative position of PM to solenoid. Fig. 6 shows variation of each coefficient according to relative position of PM to solenoid with dimensions and properties based on Section 2.3. By this, we can know the reason why the terms in object function are inserted.

The optimization was performed in terms of ADS (A Fortran Program for Automated Design Synthesis) [15]. Sequential Quadratic Programming algorithm is used to the strategy in ADS, Method of Feasible Direction to the optimizer, and Golden section method to one-dimensional search method.

Values assigned to initial parameters are mass and mass moment of inertia of system, volume of solenoid, magnetization of PM given in Table 1. Above values and minimum allowable values of stiffness coefficients are decided to prevent a thermal trouble of the solenoid due to excessive current and to reject disturbance robustly within a definite range. Optimized results are given in Table 2, and the dynamic formulations calculated by the optimized parameters are:

$$\ddot{X} + 3.6369\dot{X} + 150X = 3.4239[(I_{dm} - I_{dn}) - 2(I_{em} - I_{en}) + (I_{fm} - I_{fn})],$$

$$\ddot{Y} + 3.6369\dot{Y} + 150Y = 5.9303[(I_{dm} - I_{dn}) - (I_{fm} - I_{fn})],$$

$$\ddot{Z} + 2.8648\dot{Z} + 556.6771Z = 6.1124(I_A + I_B + I_C),$$

$$\ddot{\alpha} + 1.5286\dot{\alpha} + 150\alpha = 123.7538\left(I_A - \frac{1}{2}I_B - \frac{1}{2}I_C\right),$$

$$\ddot{\beta} + 1.5286\dot{\beta} + 150\beta = 106.4245(I_B - I_C),$$

$$\ddot{\gamma} + 7.5796\dot{\gamma} + 650.4952\gamma = -103.2034[(I_{dm} - I_{dn}) + (I_{em} - I_{en}) + (I_{fm} - I_{fn})].$$

$$(13)$$

Table 1
Basic properties and dimensions of system

Parameter	Description	Value
V_e	Volume of air-core solenoid $\pi(R^2 - r^2)l$	20.4204 cm^3
V_p	Volume of PM ($\pi 0.5^2 \times 1.0$)	0.7854 cm^3
L	Distance from D to dm	0.05 m
M	Magnetization	867 000 A/m
m	Mass of system	0.173 kg
I_{xx}	Mass moment of inertia	4.26 kg cm^2
I_{yy}	Mass moment of inertia	4.29 kg cm^2
I_{zz}	Mass moment of inertia	8.18 kg cm^2

Table 2
Optimization results of design variables

Value		
	Minimum of stiffness coefficient/Inertia property: 150	
Parameter	In-plane solenoid	Out-of-plane solenoid
Inner diameter	0.016	0.016 m
Outer diameter	0.0362	0.0367 m
Length	0.0246	0.0238 m
Nominal position	0.0151	0.0164 m
Nominal current	0.4273	0.535 A
Coil turns number	996	986
r_2	0.0715 m	0.0715 m

The above result shows that the optimized system is robust enough to resist external disturbances, then we need not take into consideration the sensitivity of any direction. Although an increase of coefficient requires more actuating power generally, the variation of the adopting point and the selection of the optimal dimension for a solenoid give us another chance to realize the effect.

4. Experimental results

A six d.o.f maglev positioner has been constructed on the basis of the optimized parameters given in the last section and is shown in Fig. 7. Different from the concept configuration (Fig. 4) in the system, there are a few holes on the levitated plate to decrease the plate weight and increase its stiffness. And this device has a docking mechanism to guarantee the repeatable initial position and rest position, and an end-pointer. As described in the figure, the spatial position and orientation of the rotor are obtained by means of optical sensors. This is accomplished by a set of three position sensors located at 120° intervals around the periphery of the
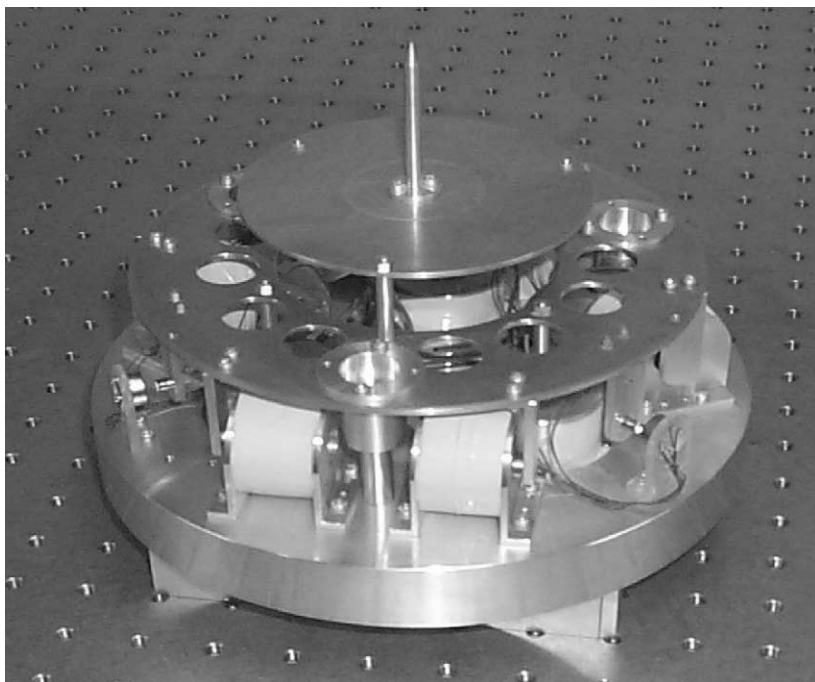
Fig. 7. The maglev positioner based on optimization.

stator's inner ring. A triplet of narrow, coplanar, radial light beams 120° apart generated by three LED projectors attached to the rotor impinge on three two-dimensional lateral effect photodiodes (it is usually called by PSD). The centroids of the light spots projected onto the active areas of the PSDs are easily obtained by measuring the current through the PSD electrodes and processing the current properly. The dynamic characteristics and performance of the system are confirmed and verified in this section. But note that the given results need to be interpreted in the context of physical characteristics of the system. Namely, the magnetic force and emf model is approximated in nature and, therefore, all results are obtained under significant parameter variation. Secondly, the optical sensors for position signal provide an accuracy of about 1 μm at a cutoff frequency of 10 Hz, which constrains the maximum accuracy and the largest bandwidth realizable from the system.

Fig. 8 shows the system block diagrams for the free vibration test and the step motion control in the z direction. Two d.o.f motions at most are controlled under closed loop, and the uncontrolled d.o.f motions are activated with just constant nominal currents. In Fig. 8, k_p, k_i, k_d represent general proportional, integral, derivative gain, respectively. Because we use gain scheduling approaches in which the nonlinear model is successively linearized at various operating points, with
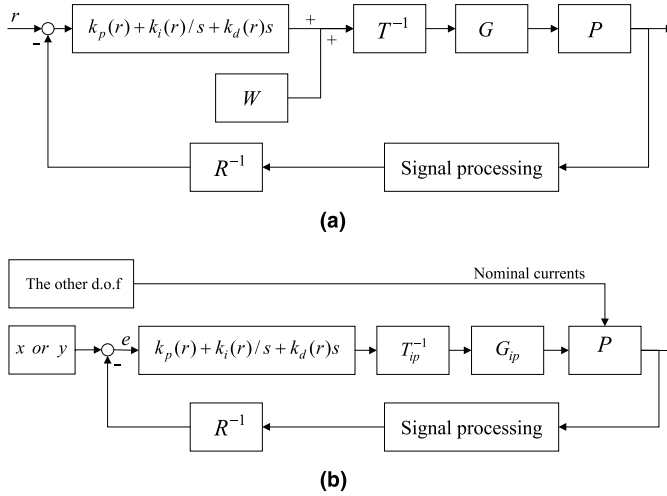
Fig. 8. Overall control block diagram (a) in case of full feedback control and (b) in case of free vibration test.

appropriate controller gains for each of these locations due to parameter variations, the above gains are functions of displacement. In the figure, W means a weight of the levitated plate, T the dynamic transform, G the servo gain array, P the plant, and R the kinematic transform.

Fig. 9 depicts the results of free vibration test performed to verify the dynamic characteristics of system, under only x motion control. The levitated moving part moves from its rest position to nominal position, arrives at steady state, and is put in motion by a small impulse. The positions of the stage are read by the optic sensors with position resolution of 1 μm. The results given in Fig. 9 are a little different from (13) because PM and solenoids used could not be identical, and the damping effects due to currents induced in the conductive rotor and solenoid bobbin are neglected. However, we have confirmed by this test that the system could keep a stable state with just a position feedback. And differences from the free vibration analysis of a perfect linear system are most likely due to severe parameter variation. Figs. 10 and 11 show the results for step motion control to quantify an influence of the uncontrolled motions on system performance. X motion is regulated at the nominal position like the above free vibration test, but z is also controlled through a conventionally linear controller. For step input of 10 μm, the gains of the linear controller are designed using the nominal model obtained by linearization at the operating point of 1 mm, whereas the response degrades for a step input of 100 μm due to parameter variations from nominal position. Then, for a step input of 100 μm, we use gain scheduling approaches in which the nonlinear model is successively linearized at various operating points, with appropriate controller gains for each of these locations [16]. Fig. 10 shows the satisfactory performance of simple linear controller. But in Fig. 11, the initial transient response degrades due to the slow
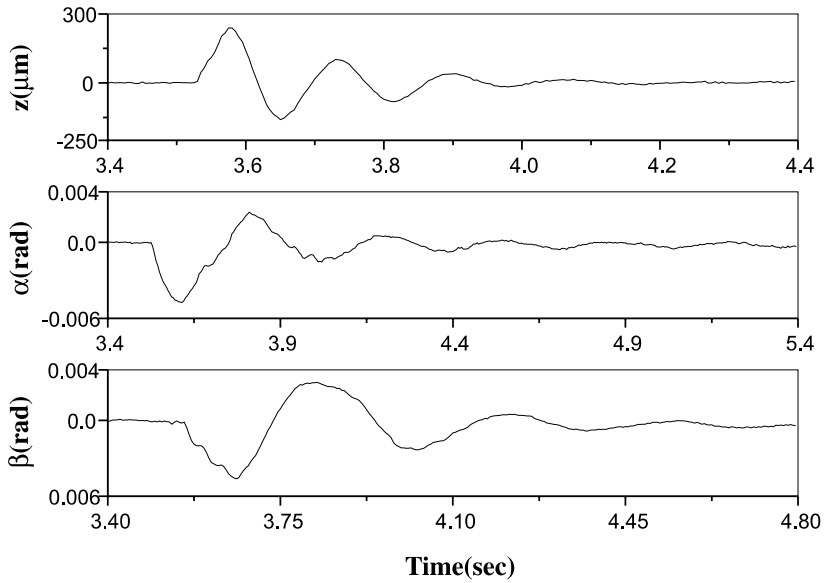
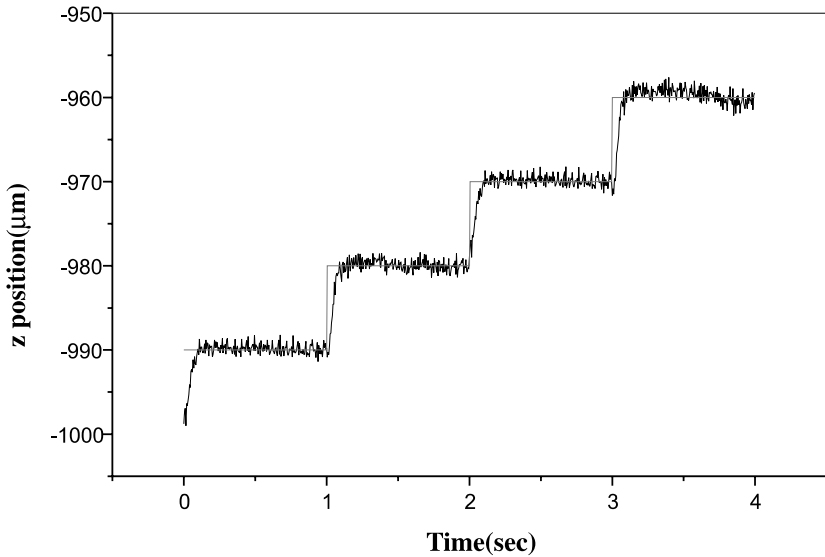Fig. 9. Free vibration analysis for the uncontrolled d.o.f.

Fig. 10. A small step input control to quantify coupling effect.

dynamics of the 10-Hz Butterworth filter incorporated into the feedback loop to eliminate sensor noise. As mentioned above, the operating range of the optic sensor
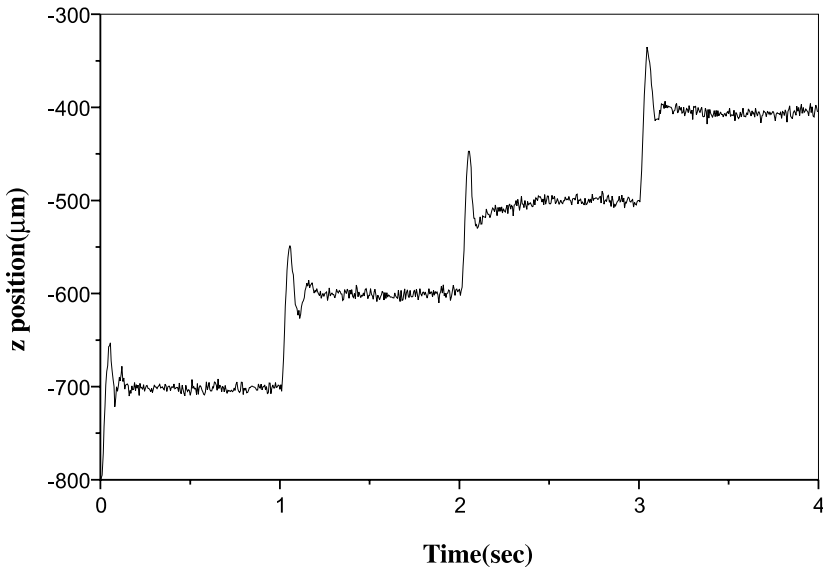
Fig. 11. A large step (100 μm) input control.

is about 4.7 mm and the A/D has 12-bit converting capability. Then, the A/D quantization level per least count is about 1 μm. But, considering the A/D converter electronics noise and quantization error, Figs. 10 and 11 represent eventually that there is little effect on system performance of motion coupling in this motion range. The results can be interpreted differently. It is that the stiffness of uncontrolled d.o.f is robust enough to neglect the coupling effect. But, as the resolution of system increases, the coupling phenomenon may be more dominant than any other factors. So it is a good issue to be studied in future, to realize nano-scale motion of the controlled d.o.f without receiving disturbance of uncontrolled motions.

5. Conclusion and future works

A six d.o.f magnetically levitated positioner, which has the self-stability for five d.o.f by just a sensory feedback in space, has been designed and demonstrated. Compared with the existing maglev positioning systems, the proposed system requires less computational load and then is able to care for performance of the only controlled motion. Using the magnetic force generated by the compounding of air core solenoid and PM and arranging the magnetic pairs properly, we could realize the system with the stability over the entire d.o.f by feedback of just a position signal.

Stiffness and damping effects of the magnetic force generated by the compounding of air core solenoids and PMs were modeled on the basis of the conventional

magnetic theory and the linearized dynamic formulations were derived. And we could maximize stiffness and damping forces of system through an optimization of solenoid dimension and its relative position to PM under the constraints of the fixed solenoid volumes and the limited currents.

Experimental results are given to confirm the validity of the design and analysis. First, free vibration test results are given to show that the system can keep the stable state with just x position feedback and to validate the dynamic characteristics. To quantify the effects on performance of controlled motion due to coupling of un-controlled motions, the step motion controls for 10 and 100 μm were tested. Although the coupling effects need not be considered in this motion range, those for nano-scale range are further issues to be studied.

Acknowledgements

References

[1] Jeong MC, Busch-Vishiniac IJ. A submicron accuracy magnetic levitation micromachine with endpoint friction. Sensors and Actuators 1991;29:225–34.

[2] Echeverria I, Rubio M. High-precision magnetic levitation device with electro-optical feedback. Rev Sci Instrum 1995;66:3931–8.

[3] Salcudean SE. A force-reflecting teleoperation system with magnetically levitated master and wrist. In: Proceedings of the IEEE International Conference on Robotics and Automation, 1992; p. 1420–6.

[4] Steve Chen SJ, Busch-Vishiniac IJ. A magnetically levitated, automated, contact analytical probe tool. IEEE Trans on Semiconductor Manufacturing 1995;8(1):72–8.

[5] Higuchi T. Magnetic supported intelligent hand for automated precise assembly. In: Proceedings of the 13th Annual IEEE Industrial Electronic Conference (IECON 87), 1987; p. 926–33.

[6] Bleuler H, Visher D. New concept for cost-effective magnetic bearing control. Automatica 1994; 30(5):871–6.

[7] Tsukamoto O, Chen JZ. A new magnetic levitation system with AC magnets. IEEE Trans Magn 1988;24(2):1497–500.

[8] Jayawant. Electromagnetic levitation and suspension techniques. London: Edward Arnold, 1981.

[9] Nakamura T. A prototype mechanism for three dimensional levitated movement of a small magnet. IEEE/ASME Trans Mechatr 1997;2(1):41–50.

[10] Hollis RL, Salcudean SE. Lorentz levitation technology: a new approach to fine motion robotics, teleoperation, haptic interface, and vibration isolation. In: Fifth International Symposium on Robotics Research, 1993.

[11] Kim WJ, Trumper DL. High-precision magnetic levitation stage for photolithography. Precis Eng 1998;22(2):66–77.

[12] Park KH, Lee SK. Contactless magnetically levitated silicon wafer transport system. Mechatronics 1996;6(5):147–56.

[13] Albert Wang IY, Busch-Vishniac IJ. A magnetic levitation transport path. IEEE Trans Semicond Manufact 1991;4(2):145–54.

[14] Wangsness Roald K. Electromagnetic fields. Chichester: Wiley; 1979.

[15] Vanderplaats GN. ADS-A Fortran Program for Automated Design Synthesis-Version 1.10. In: NASA CR-177985, 1985.

[16] Kim CY, Kim KH. Gain scheduled control of magnetic suspension systems. In: Proceedings of the American Control Conference, 1994; p. 3127–31.